https://doi.org/10.15407/ujpe71.1.15

N. KALZHIGITOV,[1] S. AMANGELDINOVA,[1] V.S. VASILEVSKY[2]

[1] Al-Farabi Kazakh National University
(71, al-Farabi Avenue, Almaty, 050040, Kazakhstan; e-mail: knurto1@gmail.com)
[2] Bogolyubov Institute for Theoretical Physics, Nat. Acad. of Sci. of Ukraine
(14b, Metrolohichna Str., Kyiv 03143, Ukraine)

STRUCTURE OF HYPERNUCLEUS ${}^{7}_{\Lambda}$Li WITHIN MICROSCOPIC THREE-CLUSTER MODEL

The structure of bound and resonance states of the hypernucleus ${}^{7}_{\Lambda}Li$ is studied within a three-cluster model. This nucleus is considered a three-cluster structure consisting of ${}^{4}He$, a deuteron, and a lambda hyperon. The chosen three-cluster configuration allows us to describe more accurately the structure of hypernucleus ${}^{7}_{\Lambda}Li$ and the dynamics of different processes that involve interactions of lightest nuclei and hypernuclei. The main goal of the present investigations is to find resonance states in the three-cluster continuum of ${}^{7}_{\Lambda}Li$ and determine their nature. A set of narrow resonance states is detected at the energy range $0 < E \leq 2$ MeV above the three-cluster threshold ${}^{4}He + d + \Lambda$.

K e y w o r d s: cluster model, resonance states, three-cluster model, hypernuclei.

1. Introduction

The physics of hypernuclear systems has a relatively long and intriguing history. The main stages of this history are discussed in detail in Refs. [1, 2]. There is a large number of experimental laboratories in the world that are trying to obtain new information on the structure of hypernuclei and their features. The geography of these laboratories and the main experimental methods they used to reveal the peculiarities of hypernuclei are presented in detail in a recently published review [3]. The main characteristics of the light hypernuclei are collected in the specialized database of hypernuclei [4]. This site displays the energies of bound states and dominant decay channels of hypernuclei.

Available experimental data stimulate a large number of theoretical investigations aimed at explaining the obtained experimental data and at predicting new features of hypernuclear systems and their interaction. Different theoretical models have been applied to study hypernuclear systems. Among them are the shell models, which described the p- and sd-shells hypernuclei [5, 6], mean-field models [7, 8], ab initio no-core shell models [9, 10], as well as numerous realizations of the cluster model [11–16]. Usually, these investigations are devoted to studying the spectra of bound states of hypernuclei. Some of these investigations, carried out within cluster models, also considered resonance states only in the two-cluster continuum.

Our attention was attracted by the ${}^{7}_{\Lambda}$Li hypernucleus. An interesting feature of the ${}^{7}_{\Lambda}$Li hypernucleus is that the spectrum consists of four bound states, exceeding the number of bound states in the ordinary ^{7}Li nucleus, which has only two bound states. There is a lack of experimental and theoretical information about resonance states in this and other hypernuclei, which decay into two or three clusters. We wish to fill this gap by employing a three-cluster microscopic model. Thus, our main aim is to detect three-cluster resonance states in the ${}^{7}_{\Lambda}$Li.

In the present work, we study the structure of both bound and resonance states of the ${}^{7}_{\Lambda}$Li hypernucleus. As we are mainly interested in the investigations of three-cluster resonance states, we adopted a three-cluster model, which was formulated in Ref. [17] and was designed to study the decay of light nuclei into three fragments (clusters). This method has

Citation: Kalzhigitov N., Amangeldinova S., Vasilevsky V.S. Structure of hypernucleus ${}^{7}_{\Lambda}$Li within microscopic three-cluster model. *Ukr. J. Phys.* **71**, No. 1, 15 (2026). https://doi.org/10.15407/ujpe71.1.15.

been successfully applied to study the structure of light atomic nuclei and especially resonance states in the three-cluster continuum of these nuclei [18–21]. Within the adopted model, the ${}^{7}_{\Lambda}$Li hypernucleus is considered as a three-cluster configuration, ^{4}He$+d+\Lambda$. The interaction of six nucleons, split into two clusters, is modeled by a semi-realistic nucleon-nucleon potential, and the sum of nucleon-hyperon potentials determines the interaction of the lambda hyperon with two clusters.

Our paper is organized as follows. In Sec. 2, we explain the key elements of our model. The main results are presented in Sec. 3. Properties of bound states are considered in Sec. 3.1. A detailed discussion of the nature of resonance states is given in Sec. 3.2. We close the paper by summarizing the obtained results in Sec. 4.

2. Method AMHHB

We shortly present the essence of the three-cluster microscopic model which is usually referred as the AMHHB model, it means the model which uses the hyperspherical harmonics basis (HHB).

We start with the seven-particle system (six nucleons and one lambda hyperon) described by a microscopic Hamiltonian. Then we reduce it to an effective three-body problem by splitting the seven particles into three groups (clusters). Then we assume that we know the wave functions describing the internal structure of each cluster with acceptable precision. Based on these assumptions, the wave function of ${}^{7}_{\Lambda}$Li is represented as

$$\Psi_J = \sum_{L,\,S} \widehat{\mathcal{A}}\Big\{\left[\Phi_1\left({}^4\mathrm{He}, S_1\right)\Phi_2\left(d, S_2\right)\Phi_3\left(\Lambda, S_3\right)\right]_S \times \times \psi_{LSJ}\left(\mathbf{x}, \mathbf{y}\right)\Big\}_J, \tag{1}$$

where $\Phi_1\left({}^4\mathrm{He}, S_1\right)$ is the wave function of an alpha particle, $\Phi_2\left(d, S_2\right)$ is the wave function of a deuteron. As the lambda hyperon is considered a structureless particle, then $\Phi_3\left(\Lambda, S_3\right)$ represents the spin part of the lambda hyperon function. The antisymmetrization operator $\widehat{\mathcal{A}}$ permutes only nucleons and, thus, makes an antisymmetric wave function of ^{6}Li, which is considered as a two-cluster system ^{4}He$+d$. Two Jacobi vectors $\mathbf{x}$ and $\mathbf{y}$ are used to determine the relative position of the clusters in the space. In what follows, the first vector $\mathbf{x}$ connects the center of masses of ^{4}He and the deuteron. In contrast, the second Jacobi vector $\mathbf{y}$ determines the relative position of the lambda hyperon regarding the center of mass of ^{6}Li.

To present the wave function of a three-cluster system (1), we use the LS coupling scheme. In this scheme, the total spin S is a vector sum of the individual spins of clusters. As the spin of ^{4}He is equal to zero, the total spin of ${}^{7}_{\Lambda}$Li is the vector sum of the deuteron spin ($S_2 = 1$) and the spin of the lambda hyperon ($S_3 = 1/2$). Thus, the total spin of ${}^{7}_{\Lambda}$Li can be $S = 1/2$ or $S = 3/2$. Within the present model, the total orbital momentum L is the vector sum of the partial orbital momenta of the relative motion of clusters (they will be introduced later), and the total momentum J is the vector sum of the total orbital momentum L and total spin S.

The wave function $\psi_{LSJ}\left(\mathbf{x}, \mathbf{y}\right)$ of the relative motion of clusters has to be determined by solving the Schrödinger equation, which is projected onto a three-cluster system and involves the selected nucleon-nucleon and nucleon-hyperon potentials. Note that the wave function $\psi_{LSJ}\left(\mathbf{x}, \mathbf{y}\right)$ depends on six variables presented by the Jacobi vectors $\mathbf{x}$ and $\mathbf{y}$. Thus, we need to introduce six quantum numbers to classify the states of a three-cluster system. By using angular orbital momentum reduction, we represent this function as

$$\psi_{LM_L}\left(\mathbf{x}, \mathbf{y}\right) \Rightarrow$$
$$\Rightarrow \sum_{\lambda,\,l} \psi_{\lambda,l;L}\left(x, y\right)\left\{Y_\lambda\left(\widehat{\mathbf{x}}\right) Y_l\left(\widehat{\mathbf{y}}\right)\right\}_{LM_L}, \tag{2}$$

where $\widehat{\mathbf{x}}$ and $\widehat{\mathbf{y}}$ are unit vectors, and λ and l are the partial angular momenta associated with vectors $\mathbf{x}$ and $\mathbf{y}$, respectively. With such a reduction, we define four quantum numbers λ, l, L and M. Within the present model, the total orbital momentum $\mathbf{L}$ is a vector coupling of partial orbital momenta $\mathbf{L} = \boldsymbol{\lambda} + \mathbf{l}$.

Wave functions of inter-cluster motion $\psi_{\lambda,l;L}\left(x, y\right)$ obey an infinite set of two-dimensional integro-differential equations. To solve this set of equations, we employ the hyperspherical coordinates and hyperspherical harmonics. There are several equivalent sets of the hyperspherical harmonics in the literature, which involve different sets of hyperspherical coordinates. We select the hyperspherical harmonics in the form suggested by Zernike and Brinkman in Ref. [22]. This form of the hyperspherical harmonics is fairly simple and does not require bulky analytical

and numerical calculations. To construct the Zernike–Brinkman hyperspherical harmonics, we need to introduce two hyperspherical coordinates ρ and θ instead of scalar coordinates x and y. The first coordinate ρ is a hyperspherical radius

$$\rho = \sqrt{x^2 + y^2}, \tag{3}$$

and the second coordinate θ is a hyperspherical angle

$$\theta = \arctan\left(\frac{x}{y}\right). \tag{4}$$

With a fixed value of ρ, this angle determines the relative length of the vectors $\mathbf{x}$ and $\mathbf{y}$

$$x = \cos\theta, \quad y = \rho\sin\theta. \tag{5}$$

One can see that the hyperradius ρ determines the size of the triangle θ which connects the centers of mass of three clusters, and the hyperangle θ determines its shape.

In new coordinates, the wave function (1) can be presented as

$$\Psi_J = \\ = \sum_{L,S}\sum_{K,\lambda,l}\widehat{\mathcal{A}}\Big\{\left[\Phi_1\left({}^4\mathrm{He}, S_1\right)\Phi_2\left(d, S_2\right)\Phi_3\left(\Lambda, S_3\right)\right]_S \times \\ \times R_c\left(\rho\right)\mathcal{Y}_c\left(\Omega\right)\Big\}_J, \tag{6}$$

where K is the hypermomentum, and $\mathcal{Y}_c\left(\Omega\right)$ stands for the product

$$\mathcal{Y}_c\left(\Omega\right) = \chi_K^{(\lambda,l)}\left(\theta\right)\left\{Y_\lambda\left(\widehat{\mathbf{x}}\right)Y_l\left(\widehat{\mathbf{y}}\right)\right\}_{LM_L} \tag{7}$$

and represents a hyperspherical harmonic for a three-cluster channel

$$c = \{K, \lambda, l, L\}. \tag{8}$$

The hyperspherical harmonic $\mathcal{Y}_c\left(\Omega\right)$ is a function of five angular variables $\Omega = \{\theta, \widehat{\mathbf{x}}, \widehat{\mathbf{y}}\}$. The definition of all components of the hyperspherical harmonic $\mathcal{Y}_c\left(\Omega\right)$ can be found, for example, in Ref. [17]. Being a complete basis, the hyperspherical harmonics account for any shape of the three-cluster triangle and its orientation. Thus, they account for all possible modes of relative motion of the three interacting clusters.

The final step toward the numerical investigation of the three-cluster system is in our hands. To simplify solving a set of integro-differential equations for hyperradial wave functions $R_c\left(\rho\right)$, we expand them over the full set of oscillator functions $\Phi_{n_\rho,K}\left(\rho, b\right)$

$$R_c(\rho) = \sum_{n_\rho,c} C_{n_\rho,c}\Phi_{n_\rho,K}(\rho, b). \tag{9}$$

As a result, a set of integro-differential equations is reduced to a system of linear algebraic equations

$$\sum_{\widetilde{n}_\rho,\widetilde{c}}\left[\langle n_\rho, c|\widehat{H}|\widetilde{n}_\rho,\widetilde{c}\rangle - E\langle n_\rho, c|\widetilde{n}_\rho,\widetilde{c}\rangle\right]C_{\widetilde{n}_\rho,\widetilde{c}} = 0, \tag{10}$$

where $\langle n_\rho, c|\widehat{H}|\widetilde{n}_\rho,\widetilde{c}\rangle$ is the matrix elements of the three-cluster Hamiltonian, and $\langle n_\rho, c|\widetilde{n}_\rho,\widetilde{c}\rangle$ is the matrix elements of the norm kernel. The oscillator function $\Phi_{n_\rho,K}\left(\rho, b\right)$ (or more precisely, the radial part of the wave function of the six-dimensional oscillator) is

$$\Phi_{n_\rho,K}\left(\rho, b\right) = (-1)^{n_\rho}\mathcal{N}_{n_\rho,K} \times \\ \times r^K\exp\left\{-\frac{1}{2}r^2\right\}L_{n_\rho}^{K+3}(r^2), \tag{11} \\ r = \rho/b, \quad \mathcal{N}_{n_\rho,K} = b^{-3}\sqrt{\frac{2\Gamma\left(n_\rho+1\right)}{\Gamma\left(n_\rho+K+3\right)}},$$

and b is an oscillator length.

System of Eqs. (10) can be solved numerically by imposing restrictions on the number of hyperradial excitations n_ρ and the number N_{ch} of hyperspherical channels $c_1,\ c_2, ..., c_{N_{\mathrm{ch}}}$. The diagonalization procedure is used to determine energies and wave functions of the bound states. However, the proper boundary conditions have to be implemented to calculate elements of the scattering S-matrix and corresponding functions of the continuous spectrum. Boundary conditions for wave functions of two- and three-body decays of a compound three-cluster system are thoroughly discussed in Refs [17, 23].

To analyze wave functions of many-channel system, obtained by solving the set of equations (10), it is expedient to combine those oscillator wave functions (11), which belong to the oscillator shell with the total number of oscillator quanta $N_{\mathrm{os}} = 2n_\rho + K$. It is then convenient to numerate the oscillator shells by quantum number $N_{\mathrm{sh}}(= 0, 1, 2, ...)$, which we determine as

$$N_{\mathrm{os}} = 2n_\rho + K = 2N_{\mathrm{sh}} + K_{\min},$$

where $K_{\min} = L$ for normal parity states $\pi = (-1)^L$ and $K_{\min} = L + 1$ for abnormal parity states

$\pi = (-1)^{L+1}$. In what follows, we will study the weights $W_{\rm sh}(N_{\rm sh})$ of oscillator wave functions of a fixed oscillator shell $N_{\rm sh}$ in the wave function of bound or continuous spectrum states. The weights $W_{\rm sh}(N_{\rm sh})$ are determined as

$$W_{\rm sh}\left(N_{\rm sh}\right) = \sum_{n_\rho, K \in N_{\rm sh}} \left|C_{n_\rho, c}\right|^2 \tag{12}$$

and indicate whether the system under consideration is compact (the oscillator shells with small values of $N_{\rm sh}$ dominate) or relatively dispersed (the oscillator shells with large values of $N_{\rm sh}$ dominate).

3. Results and Discussions

For a detailed investigation of bound and resonance states of ${}^{7}_{\Lambda}$Li, we selected the Hasegawa–Nagata potential (HNP) [24, 25] and a nucleon-hyperon potential [26], which is usually called the YNG-NF potential. The oscillator length b, which is the only free parameter of our model and which determines the distribution of nucleons inside clusters ^{4}He and d, is chosen to minimize the energy of the three-cluster threshold ${}^4\mathrm{He}+d+\Lambda$ and for the HNP, equals $b = 1.357$ fm. With this value of b, the bound state energy of ^{6}Li accounted for from the two-cluster threshold ${}^4\mathrm{He}+d$ is $E(1^+) = -1.431$ MeV, which is close to the experimental value $E(1^+) = -1.474$ MeV.

Note that with the chosen three-cluster configuration ${}^4\mathrm{He}+d+\Lambda$, we have three two-cluster subsystems ${}^4\mathrm{He}+d$, $d+\Lambda$ and ${}^4\mathrm{He}+\Lambda$. They are of importance for the present calculations. We rely on the results of Ref. [27], where the interaction of a deuteron with an alpha particle was considered, and on the results of Ref. [28], where the interaction of a lambda hyperon with a deuteron and an alpha particle was investigated in detail.

After the oscillator length b and the nucleon-nucleon (NN) and nucleon-hyperon ($N\Lambda$) potentials were selected, we need to fix another two input parameters: the number of channels or number of hyperspherical harmonics, and the number of hyper-radial excitations. We have to restrict ourselves to a finite set of hyperspherical harmonics, which is determined by the maximal value of the hyperspherical momentum $K_{\rm max}$. To describe the positive parity states, we use all hyperspherical harmonics with the hypermomentum $K \leq K_{\rm max} = 12$, and the negative parity states are represented by the hyperspherical harmonics with $K \leq K_{\rm max} = 11$. These numbers of hyperspherical harmonics allow us to describe a large number of scenarios of the three-cluster decay. We also have to restrict ourselves to the number of hyperradial excitations $n_\rho \leq 100$. This number of hyperradial excitations allows us to reach the asymptotic region, where all clusters are well separated, and the inter-cluster interaction induced by the NN or/and $N\Lambda$ potentials becomes negligibly small.

3.1. Bound states

The spectrum of ${}^{7}_{\Lambda}$Li bound states, which is obtained with the HNP and YNG potentials, is shown in Table 1. The energy of bound states is reckoned from the three-cluster threshold ${}^4\mathrm{He}+d+\Lambda$. The energies of the deeply bound $1/2^+$, $3/2^+$ and $5/2^+$, obtained with our model, are very close to the experimental values. However, our model generates the weakly bound $1/2^+$ state, which is approximately 2.1 MeV underbound. The mass root-mean-square radii R_m indicate that the deeply bound states are compact states, with $2.0 < R_m < 2.2$ fm, while the weakly bound state is a very dispersed state with a large value of $R_m = 4.5$ fm.

To understand the structure of bound states, we consider the correlation functions $D\left(x, y\right)$, which are determined as

$$D\left(x, y\right) = \left(xy\right)^2 \sum_{\lambda, l, L} \left|\psi_{\lambda, l; L}\left(x, y\right)\right|^2.$$

Note that the correlation function determines the most probable geometry (relative position) of three interacting clusters. In Fig. 1, we display a correlation function for the ground state of ${}^{7}_{\Lambda}$Li. The main peak of the correlation function corresponds to the

Table 1. **Spectrum of ${}^{7}_{\Lambda}$Li calculated with the HNP and YNG potentials**

J^π	AM HHB		Exp.
	E, MeV	R_m, fm	E, MeV
$1/2^+$	–7.060	2.183	–7.094
$3/2^+$	–6.587	2.208	–6.402
$5/2^+$	–4.856	2.036	–5.043
$1/2^+$	–1.113	4.524	–3.217
${}^4\mathrm{He}+d+\lambda$	0.0	–	0.0

three-cluster configuration where the distance between the deuteron and alpha particle is approximately 2.9 fm and the lambda particle is located close to the center of mass of ^{6}Li at a distance of 1.7 fm.

It is worthwhile noticing that the $3/2^-$ ground state of the ordinary nucleus ^{7}Li, determined with the three-cluster configuration $^4\mathrm{He} + d + n$ and with the same input parameters, has a lower bound state energy (–11.24 MeV concerning the three-cluster threshold, while the bound state energy of ${}^{7}_{\Lambda}$Li is –7.06 MeV) and it should be more compact than ${}^{7}_{\Lambda}$Li. However, the most probable distance between a deuteron and an alpha particle is $x = 3.45$ fm, and the distance between a neutron and ^{6}Li is $y = 2.05$ fm. Such distances reflect that the ground state of ^{7}Li is mainly the two-cluster configuration $^3\mathrm{H}+^4\mathrm{He}$, where the valence neutron is very close to the deuteron. (See Ref. [29] for details of such calculations.). Besides, the Pauli principle plays an important role in the formation of the bound states of ^{7}Li. The antisymmetrization over all nucleons creates the Pauli forbidden states, which are not observed in ${}^{7}_{\Lambda}$Li.

The correlation function for the $5/2^+$ excited state of ${}^{7}_{\Lambda}$Li is shown in Fig. 2. Comparing correlation functions for $5/2^+$ and $1/2^+$ states, we see that in the $5/2^+$ excited state, the lambda hyperon is rather far from ^{6}Li compared to the $1/2^+$ states. Besides, the distance between the deuteron and the alpha particle, forming ^{6}Li, is much smaller in the $5/2^+$ state than in the $1/2^+$ state. The peak of the correlation function for the $5/2^+$ state is located at $x = 1.27$ fm and $y = 2.95$ fm. It means that in this state, the distance between the deuteron and the alpha particle is almost two times smaller than in the $1/2^+$ ground state. For comparison, the distance between the lambda hyperon and ^{6}Li is approximately two times smaller.

Additional information about the peculiarities of the bound states of ${}^{7}_{\Lambda}$Li can be obtained by analyzing the weights of different oscillator shells in the wave functions of the bound states. The definition of such quantities can be found in Refs. [19–21]. In Fig. 3, the weights of different oscillator shells W_{sh} are displayed for the $1/2^+$ ground and first excited $5/2^+$ states. The largest contribution of the lowest oscillator shell $N_{\mathrm{sh}} = 0$ to the wave functions of interest indicates that the lambda hyperon with a large probability (>50%) can be found inside the nucleus ^{6}Li.

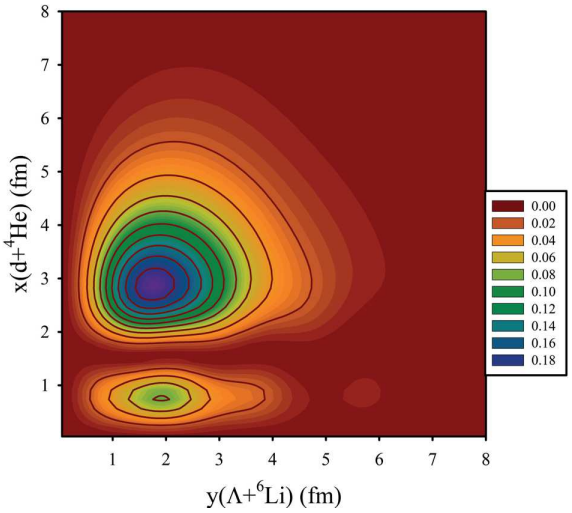

Fig. 1. Correlation function of the ${}^{7}_{\Lambda}$Li ground state as a function of distances x and y. The length of vector **x** determines the distance between the deuteron and alpha particle, and the length of vector **y** determines the distance between the lambda hyperon and the ^{6}Li

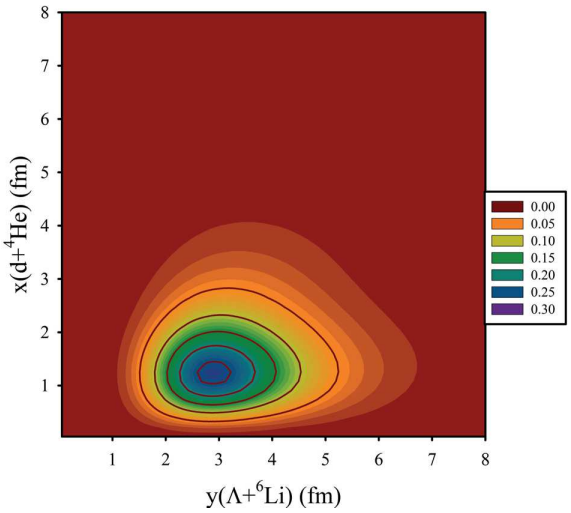

Fig. 2. Correlation function of the $5/2^+$ excited state in ${}^{7}_{\Lambda}$Li

In Fig. 4, we compare the structure of wave functions of the ground states of ^{7}Li and ${}^{7}_{\Lambda}$Li. Recall that the $3/2^-$ state is the ground state of ^{7}Li and the $1/2^+$ state represents the ground state. One can see that the lowest shell N_{sh}=0 gives zero contribution to the wave function of the ^{7}Li ground state. This shell describes the condensate of three clusters ^{4}He, d, n, and thus it is a forbidden shell for ^{7}Li due to the Pauli principle.

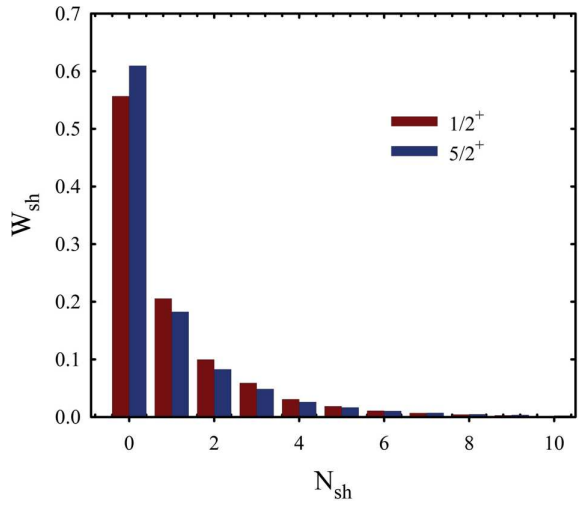

Fig. 3. Weights of different oscillator shells to the wave functions of $1/2^+$ and $5/2^+$ states in ${}^{7}_{\Lambda}$Li

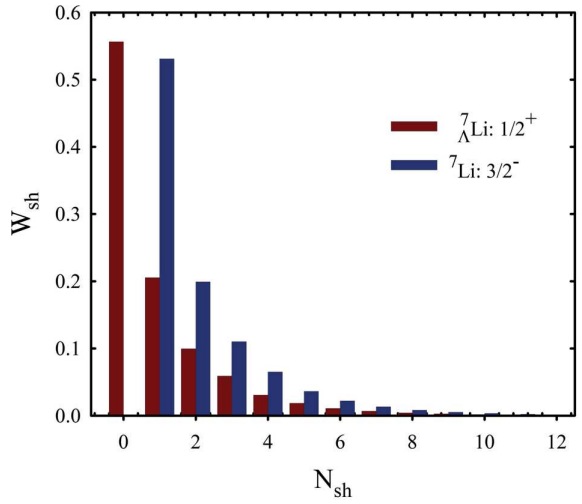

Fig. 4. Decomposition of wave functions of the ^{7}Li and ${}^{7}_{\Lambda}$Li ground states over oscillator shells

Table 2. **Parameters of resonance states found in three-cluster continuum of ${}^{7}_{\Lambda}$Li**

J^π	E, MeV	Γ, MeV	Γ/E
$5/2^+$	0.290	0.00104	3.6×10^{-7}
$1/2^-$	1.545	0.264	0.171
$3/2^-$	1.043	0.279	0.267
$3/2^-$	1.551	0.249	0.161
$1/2^+$	1.520	0.547	0.360
$3/2^+$	1.604	0.696	0.434

3.2. Resonance states

In Table 2, we collect information on resonance states of ${}^{7}_{\Lambda}$Li determined in the three-cluster continuum ^{4}He $+ d + \Lambda$. The energies of resonance states are found in the energy range from 0.2 to 2 MeV. It seems that the state $3/2^-$ generates the largest kinematical and Coulomb barrier, which resides in two resonance states with relatively small total widths Γ. The ratio Γ/E is used to distinguish very narrow, narrow and relatively wide resonance states (see, for example, Ref. [20,21]). It indicates that the $5/2^-$ resonance state with the energy $E = 0.290$ MeV is the narrow-

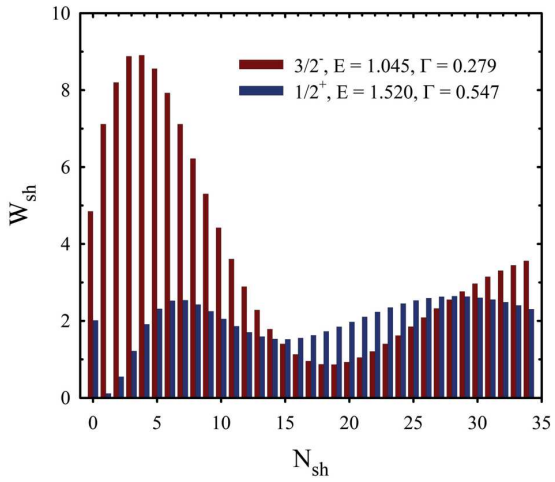

Fig. 5. Weights of the wave function of different oscillator shell in the wave functions of the $3/2^-$ and $3/2^+$ resonance states

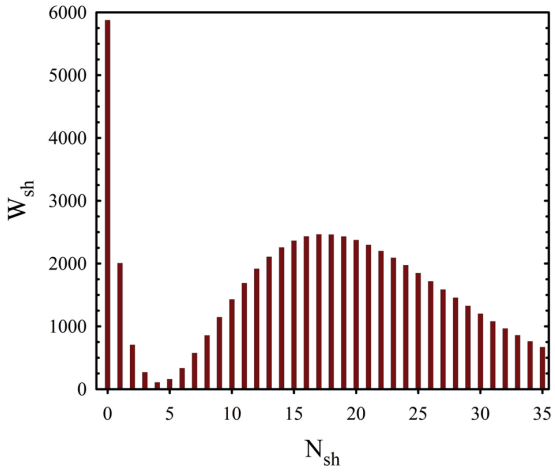

Fig. 6. Weights of different oscillator shells in the wave function of the super narrow $5/2^+$ resonance state

est resonance state (with the total width of 1.0 keV) in the three-cluster continuum of ${}^{7}_{\Lambda}$Li and the $3/2^+$ resonance state with the energy $E = 1.604$ MeV is the widest resonance state.

To understand the nature of resonance states, it is expedient to analyze resonance wave functions. In Fig. 5, the weights of different oscillator shells in wave functions of the narrowest $3/2^-$ states are compared with the weights of the widest $3/2^+$ resonance state. The wave function of a narrow resonance state has a large contribution of the oscillator shells with small values of $N_{\rm sh}$, namely, $0 \le N_{\rm sh} \le 10$. It is necessary to recall that oscillator wave functions of these shells describe the most compact three-cluster configurations. The wave function of a rather wide resonance state is spread over a large number of oscillator shells.

The structure of the wave function of the very (super) narrow $5/2^+$ resonance is shown in Fig. 6. The weights of oscillator shells in the wave function of the resonance state have much larger amplitudes. Such enormous amplitudes have been observed for the long-lived Hoyle state in ^{12}C [19] and for Hoyle-analogue states in some light nuclei [21]. It is necessary to note that 126 channels participate in the formation of the $5/2^+$ continuous spectrum states. And only one channel dominates in the decay (or formation) of the super-narrow $5/2^+$ resonance state. This channel has quantum numbers: $c = \{K = 2, l_1 = 0, l_2 = 2, L = 2, S = 1/2\}$.

4. Conclusions

We have studied the structure of the ${}^{7}_{\Lambda}$Li hypernucleus by employing a three-cluster microscopic model, which allows us to study not only bound states, but three-cluster resonance states. We have calculated energies and wave functions of bound states of ${}^{7}_{\Lambda}$Li, and revealed those channels that give the maximal contribution to the wave function of these states. We also calculated the mass root-mean-square radii of the bound states, which indicate that the hypernucleus ${}^{7}_{\Lambda}$Li is more compact than the ordinary ^{7}Li nucleus. It is shown that the present model fairly good describes the bound states of ${}^{7}_{\Lambda}$Li. It was also demonstrated that all but one bound states of ${}^{7}_{\Lambda}$Li are very compact states with small values of the mass root-mean-square radius. Correlation functions revealed the most probable relative position (distribution) of clusters in coordinate space. Besides, the weights of the functions of a fixed oscillator shell in the wave functions of the bound states of ${}^{7}_{\Lambda}$Li unambiguously demonstrate that the lambda hyperon can be located inside the nucleus ^{6}Li with significant probability.

The microscopic model we employed involves hyperspherical harmonics to numerate channels of a three-cluster system and to implement proper boundary conditions for the three-cluster continuum. This model allowed us to find a set of narrow and fairly wide resonance states in the three-cluster continuum of ${}^{7}_{\Lambda}$Li. Analysis of resonance wave functions reveals that the narrow resonance states are very compact three-cluster configurations with small distances between interacting clusters.

These results can be considered a prediction of the existence of narrow resonance states in hypernucleus ${}^{7}_{\Lambda}$Li and can be used for planning of future experiments.

This work was partially supported by the Science Committee of the Ministry of Education and Science of the Republic of Kazakhstan (Grant No. AP22683187, the project title "Structure of the light nuclei and hypernuclei in multi-channel and multi-cluster models") and by the Program of Fundamental Research of the Physics and Astronomy Department of the National Academy of Sciences of Ukraine (Project No. 0122U000889). V.V.S. is also grateful to the Simons Foundation for their financial support (Award ID: SFI-PD-Ukraine-00014580).

1. D.H. Davis. 50 years of hypernuclear physics. I. The early experiments. *Nucl. Phys. A* **754**, 3 (2005).
2. R.H. Dalitz. 50 years of hypernuclear physics. II. The later years. *Nucl. Phys. A* **754**, 14 (2005).
3. J.H. Chen, L.S. Geng, E. Hiyama, Z.W. Liu, J. Pochodzalla. Perspectives for hyperon and hypernuclei physics. arXiv:2506.00864v1 [nucl-th].
4. P. Eckert, P. Achenbach, *et al. Chart of Hypernuclides – Hypernuclear Structure and Decay Data* (2021).
5. A. Gal, J.M. Soper, R.H. Dalitz. A shell-model analysis of Λ binding energies for the p-shell hypernuclei III. Further analysis and predictions. *Ann. Phys.* **113**, 79 (1978).
6. D.J. Millener. Shell-model calculations for p-shell hypernuclei. *Nucl. Phys. A* **881**, 298 (2012).
7. N.K. Glendenning, D. von-Eiff, M. Haft, H. Lenske, M.K. Weigel. Relativistic mean-field calculations of Λ and Σ hypernuclei. *Phys. Rev. C* **48**, 889 (1993).
8. I. Vidaña, A. Polls, A. Ramos, H.J. Schulze. Hypernuclear structure with the new Nijmegen potentials. *Phys. Rev. C* **64**, 044301 (2001).

9. R. Wirth, D. Gazda, P. Navrátil, A. Calci, J. Langhammer, R. Roth. Ab initio description of p-shell hypernuclei. *Phys. Rev. Lett.* **113**, 192502 (2014).
10. H. Le, J. Haidenbauer, U.G. Meißner, A. Nogga. Jacobi no-core shell model for p-shell hypernuclei. *Eur. Phys. J. A* **56**, 301 (2020).
11. T. Motoba, H. Bando, K. Ikeda. Light p-shell λ-hypernuclei by the microscopic three-cluster model. *Prog. Theor. Phys.* **70**, 189 (1983).
12. T. Motoba, H. Bandō, K. Ikeda, T. Yamada. Chapter III. Production, structure and decay of light p-shell lambda-hypernuclei. *Prog. Theor. Phys. Suppl.* **81**, 42 (1985).
13. E. Hiyama, T. Yamada. Structure of light hypernuclei. *Prog. Part. Nucl. Phys.* **63**, 339 (2009).
14. E. Hiyama. Few-body aspects of hypernuclear physics. *Few-Body Systems* **53**, 189 (2012).
15. A.V. Nesterov, M. Solokha-Klymchak. Properties of ${}^{4}_{\lambda}$h hypernucleus in three-cluster microscopic models. *Ukr. J. Phys.* **66**, 846 (2021).
16. A.V. Nesterov, Y.A. Lashko, V.S. Vasilevsky. Structure of the ground and excited states in ${}^{9}_{\Lambda}$Be nucleus. *Nucl. Phys. A* **1016**, 122325 (2021).
17. V. Vasilevsky, A.V. Nesterov, F. Arickx, J. Broeckhove. Algebraic model for scattering in three-s-cluster systems. I. Theoretical background. *Phys. Rev. C* **63**, 034606 (2001).
18. A.V. Nesterov, F. Arickx, J. Broeckhove, V.S. Vasilevsky. Three-cluster description of properties of light neutron- and proton-rich nuclei in the framework of the algebraic version of the resonating group method. *Phys. Part. Nucl.* **41**, 716 (2010).
19. V. Vasilevsky, F. Arickx, W. Vanroose, J. Broeckhove. Microscopic cluster description of ^{12}C. *Phys. Rev. C* **85**, 034318 (2012).
20. V.S. Vasilevsky, K. Katō, N. Takibayev. Formation and decay of resonance states in ^{9}Be and ^{9}B nuclei: Microscopic three-cluster model investigations. *Phys. Rev. C* **96**, 034322 (2017).
21. V.S. Vasilevsky, K. Katō, N. Takibayev. Systematic investigation of the Hoyle-analog states in light nuclei. *Phys. Rev. C* **98**, 024325 (2018).
22. F. Zernike, H.C. Brinkman. Hypersphärische Funktionen und die in sphärische Bereichen orthogonalen Polynome. *Proc. Kon. Acad. Wetensch. Amsterdam* **38**, 161 (1935).
23. V.S. Vasilevsky, Y.A. Lashko, G.F. Filippov. Two- and three-cluster decays of light nuclei within a hyperspherical harmonics approach. *Phys. Rev. C* **97**, 064605 (2018).
24. A. Hasegawa, S. Nagata. Ground state of ^{6}Li. *Prog. Theor. Phys.* **45**, 1786 (1971).
25. F. Tanabe, A. Tohsaki, R. Tamagaki. $\alpha\alpha$ scattering at intermediate energies. *Prog. Theor. Phys.* **53**, 677 (1975).
26. Y. Yamamoto, T. Motoba, H. Himeno, K. Ikeda, S. Nagata. Hyperon-nucleon and hyperon-hyperon interactions in nuclei. *Prog. Theor. Phys. Suppl.* **117**, 361 (1994).
27. N. Kalzhigitov, N.Z. Takibayev, V.S. Vasilevsky, E.M. Akzhigitova, V.O. Kurmangaliyeva. A microscopic two-cluster model of processes in ^{6}Li. *News Nat. Acad. Scien. Rep. Kazakhstan: Phys.-Math. Ser.* **4**, 332 (2020).
28. N.K. Kalzhigitov, S. Amangeldinova, V.O. Kurmangaliyeva, V.S. Vasilevsky. Discrete and continuous spectrum of lightest hypernuclei. arXiv:2509.01932v1 [nucl-th].
29. A.V. Nesterov, V.S. Vasilevsky, T.P. Kovalenko. Effect of cluster polarization on the spectrum of the ^{7}Li nucleus and on the reaction ^{6}Li(n,^{3}H)^{4}He. *Phys. Atom. Nucl.* **72**, 1450 (2009).

Received 22.08.25

Н. Калжігітов,
С. Амангельдінова, В.С. Василевський

СТРУКТУРА ГІПЕРЯДРА ${}^{7}_{\Lambda}$Li В РАМКАХ МІКРОСКОПІЧНОЇ ТРИКЛАСТЕРНОЇ МОДЕЛІ

Зв'язані та резонансні стани гіперядра ${}^{7}_{\Lambda}$Li досліджуються в рамках трикластерної моделі. Це ядро розглядається як трикластерна структура, що складається з ^{4}He, дейтрона та лямбда-гіперона. Обрана трикластерна конфігурація дозволяє нам точніше описати структуру гіперядра ${}^{7}_{\Lambda}$Li та динаміку різних процесів, які включають взаємодію найлегших ядер та гіперядер. Головною метою даних досліджень є знаходження резонансних станів у трикластерному континуумі ${}^{7}_{\Lambda}$Li та визначення їхньої природи. У діапазоні енергій на 2 МеВ вище трикластерного порогу системи ${}^{4}\mathrm{He}+d+\Lambda$ виявлено низку вузьких резонансних станів.

Ключові слова: кластерна модель, резонансні стани, трикластерна модель, гіперядра.